Solvent-Based Soft-Patterning of Graphene Lateral Heterostructures for Broadband High-Speed Metal–Semiconductor–Metal Photodetectors

Yang Xu, Ayaz Ali, Khurram Shehzad, Nan Meng, Mingsheng Xu, Yuhan Zhang, Xinran Wang, Chuanhong Jin, Hongtao Wang, Yuzheng Guo, Zongyin Yang, Bin Yu, Yuan Liu, Qiyuan He, Xiangfeng Duan, Xiaomu Wang, Ping-Heng Tan, Weida Hu, Hai Lu, and Tawfique Hasan**

Solvents are essential in synthesis, transfer, and device fabrication of 2D materials and their functionalized forms. Controllable tuning of the structure and properties of these materials using common solvents can pave new and exciting pathways to fabricate high-performance devices. However, this is yet to be materialized as solvent effects on 2D materials are far from well understood. Using fluorine functionalized chemical vapor deposited graphene (FG) as an example, and in contrast to traditional "hard-patterning" method of plasma etching, the authors demonstrate a solvent-based "soft-patterning" strategy to enable its selective defluorination for the fabrication of graphene-FG lateral heterostructures with resolution down to 50 nm. In this strategy, the oxygen plasma etching process of patterning after graphene transfer is avoided and high quality surfaces are preserved through a physically continuous atomically thin sheet, which is critical for high performance photodetection, especially in the high-speed domain. The fabricated lateral graphene heterostructures are further employed to demonstrate a high speed metal–semiconductor–metal photodetector (<10 ns response time), with a broadband response from deep-UV (200 nm) to near-infrared (1100 nm) range. Thanks to the high quality surface with much less defects due to the "soft-patterning" strategy, the authors achieve a high deep-UV region photoresponsivity as well as the ultrafast time response. The strategy offers a unique and scalable method to realize continuous 2D lateral heterostructures and underscores the significance of inspiring future designs for high speed optoelectronic devices.

Prof. Y. Xu, A. Ali, Dr. K. Shehzad, Dr. N. Meng, Prof. M. Xu
College of Information Science & Electronic Engineering
State Key Laboratory of Silicon Materials
Zhejiang University
Hangzhou, Zhejiang 310027, China
E-mail: yangxu-isee@zju.edu.cn

Prof. Y. Xu, Z. Yang, Dr. T. Hasan
Cambridge Graphene Centre
University of Cambridge
Cambridge CB3 0FA, UK
E-mail: th270@cam.ac.uk

Y. Zhang, Prof. X. Wang, Prof. X. Wang
National Laboratory of Solid State Microstructures
School of Electronic Science and Engineering
Collaborative Innovation Center of
Advanced Microstructures
Nanjing University
Nanjing 210093, China

Prof. C. Jin
School of Materials Science and Engineering
Zhejiang University
Hangzhou, Zhejiang 310027, China

Prof. H. Wang
Institute of Applied Mechanics
Zhejiang University
Hangzhou, Zhejiang 310027, China

Dr. Y. Guo
Rowland Institute
Harvard University
100 Edwin H Land Blvd, Cambridge, MA 02142, USA

Prof. B. Yu
College of Nanoscale Science and Engineering
State University of New York
Albany, NY 12203, USA

Dr. Y. Liu, Dr. Q. He, Prof. X. Duan
Department of Chemistry and Biochemistry
and California Nanosystems Institute
University of California
Los Angeles, CA 90095, USA

Prof. P.-H. Tan
State Key Laboratory of Superlattices and Micro Structures
Institute of Semiconductors
Chinese Academy of Sciences
Beijing 100083, China

Prof. W. Hu
National Laboratory for Infrared Physics
Shanghai Institute of Technical Physics
Chinese Academy of Sciences
Shanghai 200083, China

Prof. H. Lu
Jiangsu Provincial Key Laboratory of Advanced
Photonic and Electronic Materials
School of Electronic Science and Engineering
Nanjing University
Nanjing 210093, China

DOI: 10.1002/admt.201600241

1. Introduction

Solvents are ubiquitous in processes ranging from materials synthesis to device fabrication. In the context of graphene and other 2D materials, solvents play a key part in the synthesis[1–3] (e.g., liquid-phase exfoliation) and functionalization[4] for their final applications. Even for 2D materials synthesized by dry methods such as chemical vapor deposition (CVD), solvents are essential for transfer[5] and device fabrication.[6] While the importance of solvents is widely recognized in 2D materials processing, the exact role of solvents on materials and device performances is not well understood. For example, although high quality defect-free graphene is generally thought to be unreactive toward common solvents, once in functionalized form (with hydrogen, oxygen, halogen, etc.), graphene can undergo a variety of reactions with solvents, including reduction,[7] elimination,[8] and substitution.[9] Such reactions can significantly alter the structure and properties of the functionalized graphene (FG) through change in nature and degree of functional group coverage.

FG is an important derivative of graphene due to its relatively higher thermal and chemical stability compared to its other functionalized forms.[10–12] A thorough review of FG is also recently published.[12] The binding of F radicals to graphene leads to surface activation and band gap opening,[11–13] rendering the resultant FG useful for applications ranging from as a seed layer for dielectric deposition[14,15] to as a growth precursor for synthesis of new 2D materials[16] and a building block for 2D heterostructures.[17] While FG, like some of the other functionalized graphene forms, holds great promises as a complementary material for next generation graphene-based electronics, it can readily defluorinate under humid conditions or when in contact with acetone[7,18] Such a phenomenon, considering acetone an important solvent for FG transfer and patterning process, can seriously undermine the potential of FG for widespread applications. This is because even a marginal change in the degree of fluorine coverage on graphene can turn FG from an insulator to a semiconductor or even a conductor, drastically changing the function and performance of electronic devices. Here, we report a systematic investigation on the effect of different solvents (polar and nonpolar, aqueous and organic) on the stability and defluorination of FG. Based on our results, we introduce a new solvent-based "soft-patterning" strategy to fabricate sub 50 nm lateral graphene-FG heterostructures. Such strategy offers several advantages over e-beam-based reductive patterning and plasma etch processing,[19] such as, scalability, room temperature processing, preservation of high quality surface, and avoidance of the creation of more trapping states, which are critical in high-speed photodetection. We also demonstrate successful integration of these lateral heterostructures for efficient optoelectronic devices by fabricating a state-of-the-art photodetector.

2. Results and Discussion

To explore the effect of solvents on FG, we start with the fluorination process. **Figure 1**a shows the changes in Raman signals and electrical resistivity of graphene fluorinated for different reaction times. Measurements carried out on graphene channels (L = 45 μm and W = 15 μm) show that as the fluorination time increases, the sheet resistance increases to up to 10 GΩ $\square^{-1}$, confirming increasing degree of fluorination. Changes in the Raman spectra with fluorination of graphene, such as emergence of disorder-induced D peak, changes in G, 2D peaks, and the ratio of their intensities, i.e., I(D)/I(G) and I(2D)/I(G) (Figure S1, Supporting Information) indicate successful formation of FG (see Section S1, Supporting Information, for further details). The coverage of fluorine atoms on the graphene samples is uniform, as indicated by Raman mapping conducted on the graphene channels (inset of Figure 1a). For the as-prepared FG on Cu foil, a maximum of ≈24.5% fluorinated carbon atoms are obtained, as measured by XPS (No sulfur was detected in full XPS survey spectra shown in Figure S2 (Supporting Information), confirming that the dissociated S-radicals from SF6 plasma did not react with the graphene). Normalized spectrum weight (%) is obtained using deconvoluted C1s into different components and area under the peak was used to calculate fluorinated carbon percentage using CasaXPS software. FG have three kinds of bonds (CF, CF_2, and CF_3), as shown in Figure 1b. Mainly, CF_2 and CF_3 bonds are found in the CVD grown graphene due to structural defects, grain boundaries, edges or vacancy defects during the plasma fluorination process[11,20] (see Section S2, Supporting Information, for detailed XPS analysis).

To avoid the fluorination associated damage to the Si substrate for the devices, we fluorinate the graphene on Cu or Ni foils directly, before transferring the FG sample on to the Si-based device. We find that after fluorination of CVD graphene on Ni/Cu substrates, its subsequent transfer by traditional poly(methyl methacrylate) (PMMA) method[21] and patterning alter its insulating properties. XPS measurement on the transferred FG (Figure 1c) shows a strong decrease in the intensity of F1s peak, indicating a loss of F content[18] (from 24.5% in as-prepared FG on Cu foil to 4.4%). We attribute this to the loss of the insulating properties of transferred FG. The defluorination process is likely due to the reaction between F atoms on the graphene and the solvent (acetone) used during the transfer process. The defluorination of FG is further confirmed by Auger electron mapping (AES) (see Figure S4, Supporting Information).

These results provide us impetus to study the effect of other commonly used solvents on defluorination of FG. For this purpose, as-prepared FGs on Cu foil are directly immersed in solvents, including deionized water (DIW), isopropanol (IPA), acetone, dichloromethane (DCM), and chloroform for a fixed immersion time of 30 min at room temperature. The samples are then characterized by XPS. The polarity of the solvents used is in the order of acetone > DIW > IPA > DCM > chloroform, with corresponding dipole moments of 2.88 > 1.85 > 1.66 > 1.60 > 1.04, respectively. After immersion in the solvent, XPS F1s peak intensity decreases and shifts marginally toward the lower binding energy (Figure 1d). Solvent-dependent fluorine reduction is also confirmed from the decrease of percentage of all types of carbon-fluorine bonds (CF, CF_2, and CF_3) calculated from XPS spectra (Table S1, Supporting Information). Considering the total fluorinated carbon atomic weight percentage (CF + CF_2 + CF_3) after immersion in different solvents, we further argue that FG is more reactive

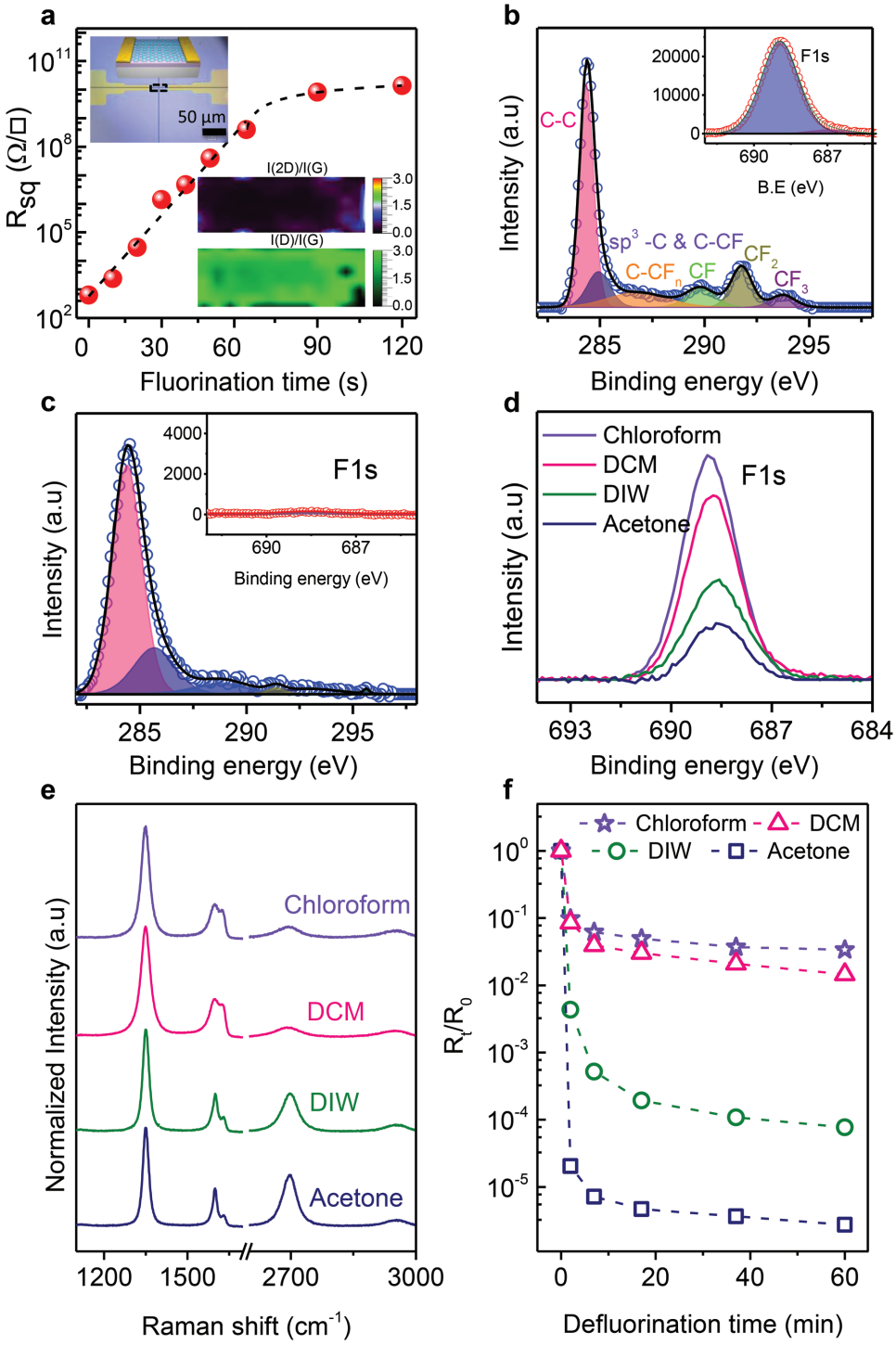

Figure 1. a) Graphene sheet resistance as the function of fluorination time, inset is an optical image and Raman mapping of an FG device channel. b) XPS spectra of as synthesized FG on Cu foil (25 W, 2 min) and c) after transfer on Si substrate. d) High resolution XPS F1s spectra of FG treated in different solvents for fixed immersion time of 30 min. e) Raman spectra of FG sample treated with solvents for 1 h. f) Normalized sheet resistance of FG devices after treatment in different solvents for various times.

and tend to defluorinate in relatively more polar solvents (see Figure S5, Supporting Information).

Raman and electrical measurements also corroborate the observation on solvent polarity-dependent defluorination of FG in solvents. For the same immersion time (1 h), defluorination induced Raman changes including the recovery of intensity of 2D peak $I(2D)$, decrease in intensity of D peak $I(D)$, and reduction of full width at half maximum of all the specified peaks

are more prominent in the relatively more polar solvents. For example, Figure 1e clearly shows a much more prominent 2D peaks in acetone treated sample compared to that from the chloroform treated sample (more details on the effect of solvent polarity and immersion time on defluorination of FG can be found in Section S6, Supporting Information). Similarly, the change in normalized sheet resistance for devices immersed in relatively polar solvent (acetone) for 60 min is more than five orders of magnitude, while it is less than approximately two orders of magnitude for devices immersed in relatively less (non) polar solvent (chloroform) for the same period (Figure 1f and Figures S7 and S10, Supporting Information). To further study the electron transport mechanism, we tested the sheet resistance of FG devices under different temperature environment, ranging from 50 to 300 K with steps of 25 K (Figure S8, Supporting Information). The as prepared FG device and FG immersed in less-polar solvents such as DCM shows insulating type behavior, with sheet resistance increasing with the decrease in temperature, an indication of hopping/tunneling between impurity states.[10] However, the FG device treated with highly polar solvent (acetone) recovers graphene like behavior (due to the removal of F atoms), where the sheet resistance increases with increasing temperature.[22] Ab initio molecular dynamics (MD) simulation in **Figure 2**a–c also confirm that relatively more polar solvents such as DIW, acetone, and IPA can completely or partially remove the F atoms, while less polar chloroform does not interact with it. This is in agreement with our experimental observations.

We argue that defluorination of FG in solvents does not take place via generally considered S_N1 and S_N2 nucleophile substitution reaction,[9] as schematically shown in Figure 2d. This is because substituting one functional group with another would not change the density of sp^3 or sp^2 carbon centers on graphene basal plane, and therefore, leading to no major change in conductivity. However, our results exhibit significant changes in electrical conductivity upon defluorination, implying that F is removed, not substituted. This is also confirmed by ab initio MD simulation, as discussed above. Removal of F would increase the density of sp^2 centers on graphene basal plane (Figure S6, Supporting Information) and allow partial restoration of the electrically conducting conjugation networks. Moreover, XPS results of defluorinated graphene do not show the presence of any new element on graphene, further supporting our conclusion that F removal/elimination[8] is the more plausible mechanism of defluorination. However, it is challenging to confirm the fate of the removed F radicals/atoms as their concentration is too low to be detected by commonly used analytical methods. Our gas chromatography-mass spectrometry characterization of the solvent (acetone) after reaction with as prepared FG sample did not detect any fluorine. In addition, ascertaining the exact mechanism is further complicated due to the lack of a clear understanding of the structure of FG itself.[7,18,23]

Based on our observations from the solvents studied, we predict that in general all the solvents high on polarity index will tend to defluorinate FG, while solvents on low polarity index will mostly be unreactive and suitable for preserving the structure and properties of FG. With rapid expansion of research and application of 2D materials, studies on the structure and properties of their functionalized forms will also expand.[24] We believe that insight into the effect of solvents obtained here will also be helpful for synthesis, property characterization, and applications of functionalized forms of the other 2D materials.

The ability of polar solvents to effectively remove fluorine atoms opens a new pathway to fabricate graphene-FG lateral heterostructures by using polar solvents as a tool to selectively defluorinate FG. Here, we demonstrate photolithography patterned graphene-FG structures from preprepared FG film on SiO_2 substrate. We achieve this by selectively exposing areas of FG to DIW for 1 h. The formation of graphene-FG lateral heterostructures is confirmed by AES mapping. The intensity distribution of F KLL Auger electron mapping clearly shows the formation of graphene-FG lateral heterostructures (Figure 2e–g) where the intensity of F KLL signal on FG area is much higher than that on the defluorinated area (and vice versa in C KLL Auger electron mapping). To further test the limit of our approach in terms of achieving various shape and size of patterned structures, we perform e-beam lithography and solvent assisted defluorination to fabricate graphene nanoribbons in graphene-FG lateral heterostructures, with widths ranging from few micrometers to sub 50 nm, as illustrated in scanning electron microscope (SEM) images in Figure 2h. The light gray and dark colors in Figure 2h represent the FG and graphene regions, respectively.[25]

The lateral graphene-FG heterostructures fabricated using our solvent assisted selective defluorination strategy are expected to provide several advantages. First, as we have demonstrated, the size and shape of the alternating regions of FG and graphene can be readily designed via lithography. Second, these heterostructures can be easily transferred[26] on to both flexible and nonflexible substrates for further applications (Figure S11, Supporting Information). Third and more importantly, the film with FG and graphene patterns is continuous with seamless boundaries between alternating graphene-FG structures, avoiding edges with dangling bonds and entanglements of micro/nanoribbons. Lastly, the boundary between FG and graphene is robust and chemically well-defined through the sp^3 C—F bonds. This is a significant advantage over the graphene ribbons using conventional methods by oxygen plasma etching, which would include mixed sp^2 and sp^3 carbon bonds anchored with a variety of functional groups, compromising the device properties.

During the preparation of our manuscript, we came across a recently published work on solvent effect on the defluorination of ultrasonically dispersed spongy graphene.[27] However, the scope of our work is fundamentally different as we focus on CVD graphene with systematic investigation and characterization, and more importantly, demonstrate an exciting new strategy to exploit the solvents as a tool for the fabrication of unprecedentedly high resolution lateral 2D heterostructures on continuous films for their use in high performance optoelectronic devices (as discussed below).

As a demonstration of our lateral graphene-FG heterostructures for applications in high performance optoelectronic devices, we fabricate an interdigitated (IDT) Gr/Si/Gr (metal–semiconductor–metal) Schottky photodetector with equally spaced 10 μm wide graphene-FG fingers (device "GR-FG") formed by selective-area defluorination using photolithography (**Figure 3**a and Figure S12, Supporting Information). We first

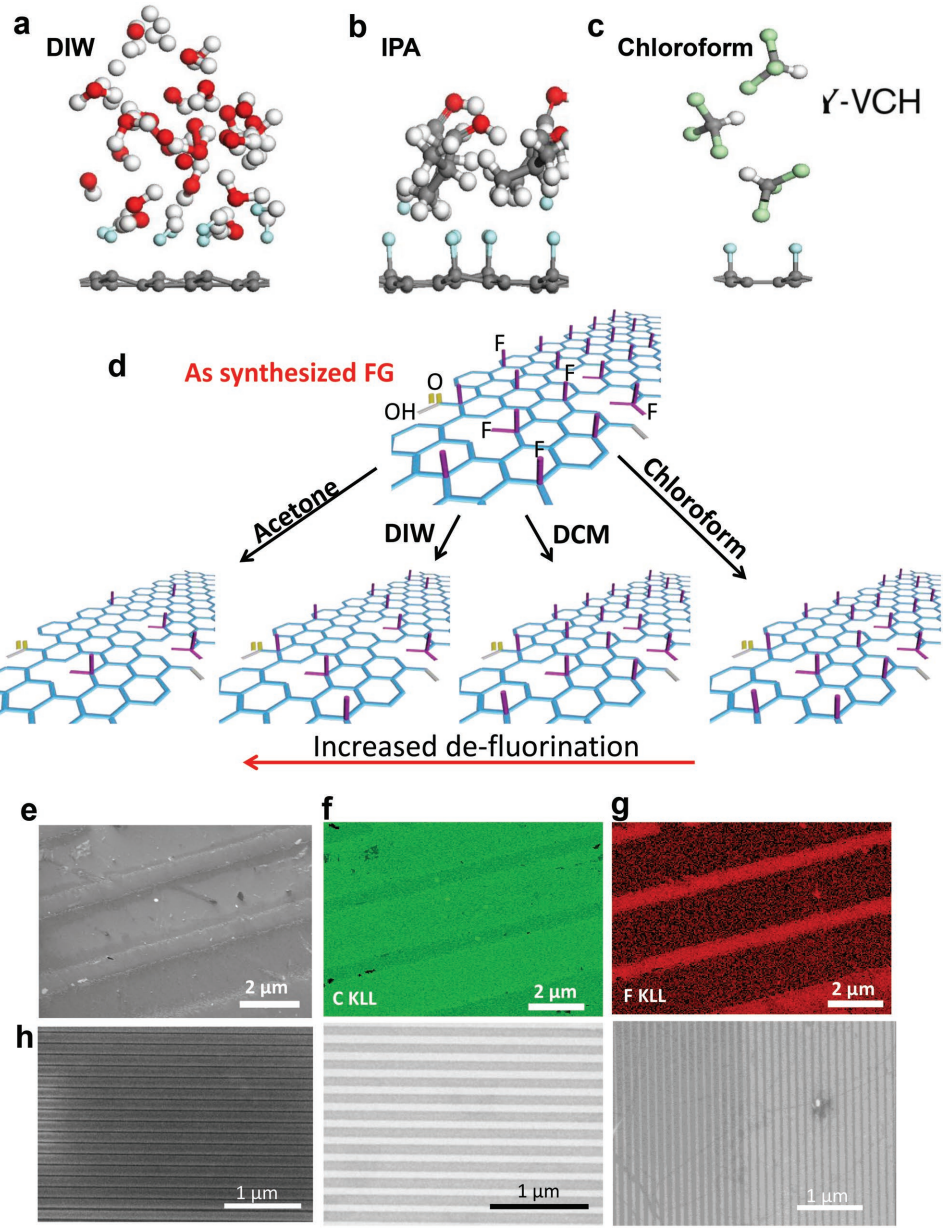

Figure 2. a–c) Typical ab initio MD snapshots of the defluorination process after 0.2 ns simulation run. Carbon, hydrogen, oxygen, fluorine, and chlorine atoms are represented as gray, white, red, cyan, and green balls, respectively. The simulation shows that a) DIW can completely remove the F atoms from the FG. b) IPA can remove a fraction of F atoms. c) Chloroform is inert and does not interact with the FG. d) Schematic of as-synthesized FG and degree of defluorination in the solvents studied here. e) SEM image of graphene and FG lateral heterostructure. f,g) AES mapping of C KLL and F KLL signals, respectively. h) SEM images graphene nanoribbons with varying ribbon width obtained using selective area defluorination of FG in DIW for 1 h.

compare the GR-FG device with a reference metal–semiconductor–metal lateral graphene photodetector (device "GR"), having the same geometrical structure with 10 μm wide graphene ribbon where the FG regions are etched away by oxygen plasma. To compare, for some devices, we also transfer an FG layer on the top of the GR-FG lateral heterostructures. Since FG is sensitive/reactive in ambient conditions,[18] we coat a 50 nm thick protective layer of aluminum oxide (Al_2O_3) on top to improve the stability of the FG devices. The dark currents decrease from ≈0.7 μA cm^{-2} for the reference GR to ≈0.4 μA cm^{-2} for GR-FG devices (Figure 3b). On the other hand, the photoresponsivity at –0.5 V bias increases from 0.13 A W^{-1} for the GR device to 0.22 A W^{-1} for the GR-FG device under an ultraviolet 375 nm laser illumination, showing an improvement of almost 160%. The obtained responsivity curves of GR and GR-FG are nearly identical in shape (Figure 3c). However, the maximum responsivity at the wavelength of ≈890 nm increases from 0.43 to 0.48 A W^{-1} for GR and GR-FG-based devices. The responsivity change is more significant for shorter wavelengths (<890 nm) than those for the longer wavelengths. We note that the shorter wavelength is more sensitive to the surface states of lateral heterostructure.We argue that since our devices have

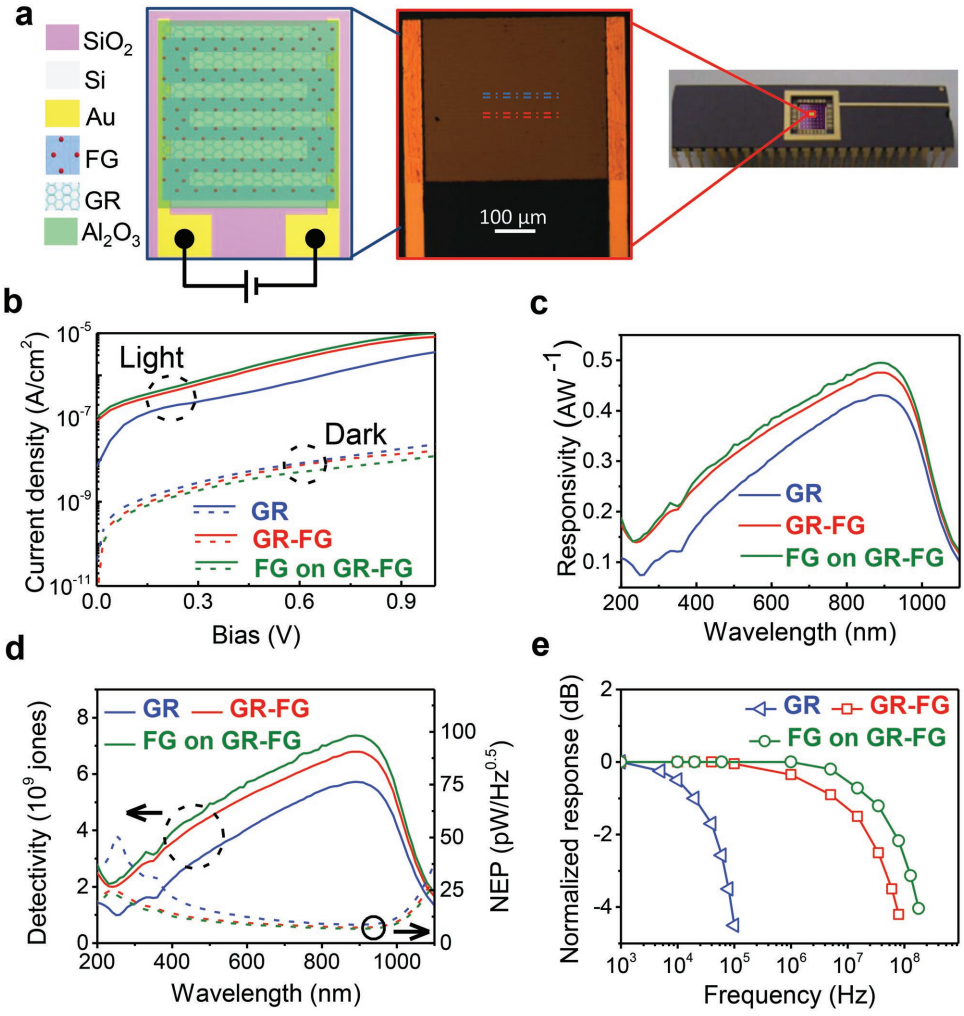

Figure 3. a) Schematics, optical image, and photograph of photodetector arrays of interdigitated (IDT) lateral patterned photodetector fabricated using selective-area defluorination of posttransferred monolayer FG on Si. b) The dark currents of the three photodetectors (dotted lines) and their photocurrents (solid lines) are compared. c) Responsivity of the three lateral photodetectors, namely, GR, GR-FG, and FG on GR-FG. d) Noise-equivalent-power (NEP) and specific detectivity of the GR, GR-FG, and FG on GR-FG photodetectors. e) Frequency response of the photodetectors based on etched Gr ribbons (blue line), GR-FG lateral heterostructures (red lines), and FG transferred upon GR-FG device (dark green).

much improved surface quality due to solvent-based defluorination, the responsivity at the shorter wavelengths is better than the longer wavelengths. Figure 3d shows that the noise-equivalent power (NEP) and corresponding specific detectivity of the GR-FG photodetector is improved by more than 60% on average (<890 nm) compared to the reference GR photodetector. Importantly, our devices after Al_2O_3 coating showed a stable performance even after one year (Figure S13, Supporting Information). We have used a pulsed laser to investigate the response time of the GR-FG photodetector. **Figure 4**a shows the time-dependent behavior of the incident pulsed laser and the photocurrent of the photodetector. The zoom-in view of a laser pulse (Figure 4b) shows that the pulse width is ≈5 ns. The rise and fall time of the pulse are both <2 ns, which qualifies our detectors as ultrafast, capable of operating to up to the GHz frequency range. Comparatively, GR device shows much shower response, even at the frequency as low as 10 kHz (Figure S14, Supporting Information). Indeed, our FG-GR lateral heterostructure photodetector qualifies all the parameters of a high performance photodetector with photocurrent NEP ≈ 7.3 pW $Hz^{-0.5}$, specific detectivity (D^*) ≈ 6.7×10^9 Jones and more importantly, <10 ns response time and >90 dB linear-dynamic region. We note that our FG-GR lateral photodetector has marginally larger dark current density and lower specific detectivity compared to previous works.[28–30] This is because relatively large leakage current is commonly observed in metal–semiconductor–metal photodetector architectures.[31] Generally, different wavelength regimes are detected by separate photoactive semiconductors with appropriate bandgaps. However our devices demonstrate consistent performance across the broad spectral range from deep ultraviolet (200 nm) to near-infrared (1100 nm). Moreover, fast time response (<10 ns) of our devices in this broad range also outperform most of the previously reported graphene Schottky free-space (non-waveguide) UV photodetectors. A comparison with reported devices is presented in Table S2 (Supporting Information). We also note that

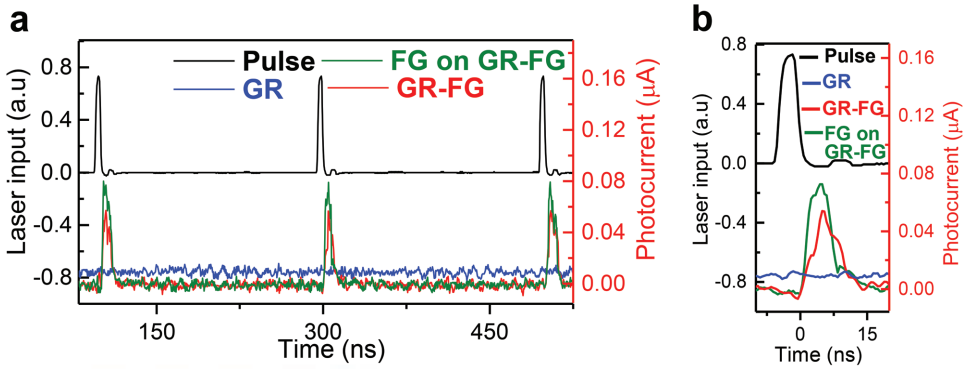

Figure 4. a) Time-dependent behavior of the incident laser light and the photocurrent of the three lateral photodetectors, namely, GR, GR-FG, and FG on GR-FG. b) Zoom-in view of a laser pulse and the time-dependent photocurrent of the three lateral photodetectors, namely, GR, GR-FG, and FG on GR-FG, responding to single laser pulse. The response speed is improved from GR to GR-FG by approximately three orders, supporting the advantages of "soft-patterning" strategy based on selective defluorination.

the device structures reported here are different from our previous work[28] on vertical graphene/Si heterostructures, where electrons and holes are collected by graphene and bulk silicon, respectively. In contrast, the device reported here are based on interdigitated patterned lateral graphene/Si/graphene heterostructures, which is very sensitive to the surface states, especially at the UV region and in the high speed domain. This is because both electrons and holes are collected by the surface graphene electrodes.

We attribute the origin of the performance improvement in responsivity, response time, and NEP to the continuous graphene-FG film fabricated by our soft-patterning strategy (room temperature defluorination by solvent) with seamless boundaries. This not only avoids the scattering and recombination effects arising from dangling bonds (present in oxygen etched graphene ribbons) but also maximizes the effective detection area in IDT devices, desirable for high performance optoelectronic applications of 2D/3D van der Waals heterostructures. In comparison, the traditional subtractive lithography (hard-patterning) needs etching or/and ion bombardment.[31] This significantly damages the van der Waals 2D heterostructures or degrades the surface quality of the underlying 3D substrate, leading to a large amount of surface trapping states and subsequent deterioration of the device performance in the high-speed domain, as shown in our GR Schottky photodetectors. We emphasize that in the deep-UV region, due to the low penetration depth of the UV light (≈10 nm), defects in graphene and Si interface could hinder the electron–hole pair separation, which can seriously limit the responsivity of photodetectors. However, for our devices, again thanks to the high quality surface with much less defects obtained by soft-patterning strategy, we achieved a very high deep-UV region photoresponsivity as well as the ultrafast time response. We find that transferring another layer of FG on top of the GR-FG lateral Schottky photodetector (denoted as "FG on GR-FG" device) further improves the Schottky junction characteristics and overall performance of the photodetector (responsivity ≈0.5 A W^{-1}, NEP ≈ 6.7 pW $Hz^{-0.5}$, D^* ≈ 7.4 × 10^9 Jones. We attribute this improvement to two factors. First, transferring FG upon the GR-FG device improves the conformal coverage of the lateral graphene-FG film on the silicon surface. This likely reduces the inhomogeneity of graphene/Si contact region. Second, high electronegativity of fluorine atoms results in charge transfer between the top FG and the bottom graphene sections of graphene-FG layer. We propose that this charge transfer enhances the p-type doping of the bottom graphene, improving the Schottky characteristics of the Graphene/Si junction. Such improvement of the junction quality with the integration of 2D graphene-FG heterostructures may offer a very effective strategy to engineer highly efficient optoelectronic devices.

3. Conclusions

We demonstrate that polar solvents, with their effective defluorination of FG, can be used as a tool for selective defluorination and therefore "soft-patterning" of high resolution graphene-FG lateral heterostructures on continuous atomically thin sheets. In our "soft-patterning" strategy (selective defluorination by solvent), the oxygen plasma etching process is avoided and high quality surfaces (the CVD monolayer graphene and the naked silicon surface) and edges are preserved through a physically continuous atomically thin sheet. This is critical for high performance optoelectronic applications using 2D/3D van der Waals heterostructures, especially in the high-speed domain. Such an outcome can be very important for next-generation 2D material-based devices, as exemplified by our state of the art photodetector with outstanding performances in terms of ultrafast time response and high responsivity in deep UV.

4. Experimental Section

Details are provided in the Materials and Methods Section of the Supporting Information.

High quality monolayer CVD grown graphene was fluorinated by gentle remote plasma fluorination. Remote plasma fluorination of graphene, under different plasma power and reaction times, was monitored by Raman, XPS, and electrical measurements. To check the effect of solvents, FG on Cu was immersed in various solvents for different durations. For photodetector fabrication, FG was transferred on prepared devices. Selective areas of FG on device were masked by spin coated PMMA and e-beam lithography. The exposed areas

were dipped in solvents to selectively defluorinate the FG for the fabrication of lateral heterostructures. XPS, SEM, AES, and Raman characterizations were performed for structural characterizations of FG and lateral heterostructures. Electrical and optoelectrical measurements were performed on Agilent semiconductor device analyzer (B5100A), Keithley Source Meter 2450, and Thorlabs lasers with 375 and 532 nm wavelengths. The response time was measured by using trans-impedance amplifier (FEMTO DHPCA-100), periodic pulse laser (Edinburgh Instruments Ltd., EPL-Series, 375 and 470 nm), and an Agilent oscilloscope (DSO 9404A, 4 GHz).

Supporting Information

Supporting Information is available from the Wiley Online Library or from the author.

Acknowledgements

Y.X., A.A., and K.S. contributed equally to this work. The authors would like to thank Prof. Erping Li, Prof. Wenyan Yin and Prof. Cheng-Te Lin for helpful discussion and comments. This work was supported by National Science Foundation of China (Grant No. 61674127, 61274123, 61474099, 21325417, 51533008 and Key Project No. 61431014), US National Science Foundation (EFRI-1433541), and micro-/nano-fabrication platform of Zhejiang University, National Key Research and Development Program (2016YFA0200200), NSFC of Zhejiang Province (Grant No. LZ17F040001, LR12F04001), National postdoc Foundation of China (2015M571868), and the Fundamental Research Funds for the Central Universities (2016XZZX001-05). This work is also supported by ZJU Cyber Scholarship and Cyrus Tang Center for Sensor Materials and Applications, the Open Research Fund of State Key Laboratory of Bioelectronics, Southeast University, the Open Research Fund of State Key Laboratory of Nanodevices and Applications at Chinese Academy of Sciences (No. 14ZS01), and a visitng By-Fellowship of Churchill College at University of Cambridge. T.H. acknowledges support from a Royal Academy of Engineering Research Fellowship (Graphlex).

Received: October 17, 2016
Revised: November 3, 2016
Published online: December 23, 2016

[1] K.-G. Zhou, N.-N. Mao, H.-X. Wang, Y. Peng, H.-L. Zhang, *Angew. Chem., Int. Ed.* **2011**, *50*, 10839.
[2] T. Hasan, F. Torrisi, Z. Sun, D. Popa, V. Nicolosi, G. Privitera, F. Bonaccorso, A. C. Ferrari, *Phys. Status Solidi* **2010**, *247*, 2953.
[3] J. N. Coleman, *Adv. Funct. Mater.* **2009**, *19*, 3680.
[4] C. Backes, N. C. Berner, X. Chen, P. Lafargue, P. LaPlace, M. Freeley, G. S. Duesberg, J. N. Coleman, A. R. McDonald, *Angew. Chem., Int. Ed.* **2015**, *54*, 2638.
[5] Y. Kim, H. Kim, T. Y. Kim, S. H. Rhyu, D. S. Choi, W. K. Park, C.-M. Yang, D. H. Yoon, W. S. Yang, *Carbon* **2015**, *81*, 458.
[6] Z. Cheng, Q. Zhou, C. Wang, Q. Li, C. Wang, Y. Fang, *Nano Lett.* **2011**, *11*, 767.
[7] J. H. Lee, G. K. W. Koon, D. W. Shin, V. E. Fedorov, J.-Y. Choi, J.-B. Yoo, B. Özyilmaz, *Adv. Funct. Mater.* **2013**, *23*, 3329.
[8] K. E. Whitener, R. Stine, J. T. Robinson, P. E. Sheehan, *J. Phys. Chem. C* **2015**, *119*, 10507.
[9] M. S. Dubecký, E. Otyepková, P. Lazar, F. E. Karlický, M. Petr, K. R. Čépe, P. Banáš, R. Zbořil, M. Otyepka, *J. Phys. Chem. Lett.* **2015**, *6*, 1430.
[10] R. R. Nair, W. Ren, R. Jalil, I. Riaz, V. G. Kravets, L. Britnell, P. Blake, F. Schedin, A. S. Mayorov, S. Yuan, *Small* **2010**, *6*, 2877.
[11] J. T. Robinson, J. S. Burgess, C. E. Junkermeier, S. C. Badescu, T. L. Reinecke, F. K. Perkins, M. K. Zalalutdniov, J. W. Baldwin, J. C. Culbertson, P. E. Sheehan, *Nano Lett.* **2010**, *10*, 3001.
[12] W. Feng, P. Long, Y. Feng, Y. Li, *Adv. Sci.* **2016**, *7*, 1500413.
[13] O. Leenaerts, H. Peelaers, A. D. Hernández-Nieves, B. Partoens, F. M. Peeters, *Phys. Rev. B* **2010**, *82*, 195436.
[14] H. Guo, Y. Liu, Y. Xu, N. Meng, H. Wang, T. Hasan, X. Wang, J. Luo, B. Yu, *Nanotechnology* **2014**, *25*, 355202.
[15] X. Zheng, M. Zhang, X. Shi, G. Wang, L. Zheng, Y. Yu, A. Huang, P. K. Chu, H. Gao, W. Ren, Z. Di, X. Wang, *Adv. Funct. Mater.* **2015**, *25*, 1805.
[16] V. Urbanova, K. Hola, A. B. Bourlinos, K. Cepe, A. Ambrosi, A. H. Loo, M. Pumera, F. Karlicky, M. Otyepka, R. Zboril, *Adv. Mater.* **2015**, *27*, 2305.
[17] A. Geim, I. Grigorieva, *Nature* **2013**, *499*, 419.
[18] R. Stine, W.-K. Lee, K. E. Whitener, J. T. Robinson, P. E. Sheehan, *Nano Lett.* **2013**, *13*, 4311.
[19] F. Withers, T. H. Bointon, M. Dubois, S. Russo, M. F. Craciun, *Nano Lett.* **2011**, *11*, 3912.
[20] B. Wang, J. Wang, J. Zhu, *ACS Nano* **2014**, *8*, 1862.
[21] J. W. Suk, A. Kitt, C. W. Magnuson, Y. Hao, S. Ahmed, J. An, A. K. Swan, B. B. Goldberg, R. S. Ruoff, *ACS Nano* **2011**, *5*, 6916.
[22] K. Tahara, T. Iwasaki, S. Furuyama, A. Matsutani, M. Hatano, *Appl. Phys. Lett.* **2013**, *103*, 143106.
[23] D. O'Hagan, *Chem. Soc. Rev.* **2008**, *37*, 308.
[24] S. Lei, X. Wang, B. Li, J. Kang, Y. He, A. George, L. Ge, Y. Gong, P. Dong, Z. Jin, *Nat. Nanotechnol.* **2016**, *11*, 465.
[25] Y. Wang, Y. Shen, X. Zhang, Y. Zhang, J. Hu, *Appl. Phys. Lett.* **2014**, *105*, 233107.
[26] H. Li, J. Wu, X. Huang, Z. Yin, J. Liu, H. Zhang, *ACS Nano* **2014**, *8*, 6563.
[27] X. Wang, W. Wang, Y. Liu, M. Ren, H. Xiao, X. Liu, *Phys. Chem. Chem. Phys.* **2016**, *18*, 3285.
[28] T. Yu, F. Wang, Y. Xu, L. Ma, X. Pi, D. Yang, *Adv. Mater.* **2016**, *28*, 4912.
[29] L.-B. Luo, L.-H. Zeng, C. Xie, Y.-Q. Yu, F.-X. Liang, C.-Y. Wu, L. Wang, J.-G. Hu, *Sci. Rep.* **2014**, *4*, 3914.
[30] X. Li, M. Zhu, M. Du, Z. Lv, L. Zhang, Y. Li, Y. Yang, T. Yang, X. Li, K. Wang, H. Zhu, Y. Fang, *Small* **2016**, *12*, 595.
[31] Y. An, A. Behnam, E. Pop, A. Ural, *Appl. Phys. Lett.* **2013**, *102*, 013110.